Metal Nanocrystal-Embedded Hollow Mesoporous TiO_2 and ZrO_2 Microspheres Prepared with Polystyrene Nanospheres as Carriers and Templates

*Zhao Jin, Feng Wang, Feng Wang, Junxin Wang, Jimmy C. Yu, and Jianfang Wang**

Noble metal nanocrystals with different shapes and compositions are embedded in hollow mesoporous metal oxide microspheres through an ultrasonic aerosol spray. Polystyrene (PS) nanospheres are employed simultaneously as a hard template to create hollow interiors inside the oxide microspheres and as the carrier to bring pregrown metal nanocrystals, including Pd nanocubes, Au nanorods, and Au core/Pd shell nanorods, into the oxide microspheres. Calcination removes the PS template and causes the metal nanocrystals to adsorb on the inner surface of the hollow oxide microspheres. The catalytic performances of the Pd nanocube-embedded TiO_2 and ZrO_2 microspheres are investigated using the reduction of 4-nitrophenol as a model reaction. The presence of the mesopores in the oxide microspheres allows the reactant molecules to diffuse into the hollow interiors and subsequently interact with the Pd nanocubes. The embedding of the metal nanocrystals in the hollow oxide microspheres prevents the aggregation of the metal nanocrystals and reduces the loss of the catalyst during recycling. The Pd nanocube-embedded ZrO_2 microspheres are found to exhibit a much higher catalytic activity, a much larger catalytic reaction rate, and a superior recyclability in comparison with a commercial Pd/C catalyst. This preparation approach could potentially be utilized to incorporate various types of mono- and multimetallic nanocrystals with different sizes, shapes, and compositions into hollow mesoporous oxide microspheres. Such a capability can facilitate the studies of the catalytic properties of various combinations of metal nanocrystals and metal oxide supports and therefore guide the design and creation of high-performance catalysts.

1. Introduction

Colloidal noble metal nanocrystals have recently received wide attention for their catalytic applications, owing to their synthetically controlled sizes, shapes, facets, and chemical compositions.[1–4] For instance, the surface areas of spherical metal catalysts are inversely proportional to their sizes. The morphology of metal nanocrystals decides the exposed facets, and therefore determines the surface activity and selectivity.[5–9] Moreover, bimetallic nanocrystals can have their *d*-band center adjusted by varying the chemical composition to be closer to the Fermi level than monometallic ones.[10] These bimetallic nanocrystals tend to exhibit high activities towards O_2 reduction reaction.[11–13] During liquid-phase catalytic reactions, colloidal metal nanocrystals are easy to aggregate or reshape owing to the change in the solvent dispersion properties or the loss of the stabilizing surfactants or polymers. In order to increase the stability of metal nanocrystal catalysts in solutions, polymers,[14,15] dendrimers,[16] resins,[17] and metal oxides[18–22] have been employed to coat, embed, or support them. Encapsulated metal nanocrystals are immobilized or confined in a small volume. They are protected and therefore less prone to aggregation and reshaping. Silica is one of the most intensively studied materials as the support for metal nanocatalysts,[18,19] due to its low cost and well-known hydrolysis and condensation chemistry. However, transition metal oxides play important roles as catalyst supports in the petrochemical industry and in automobile exhaust emission control, because they are more chemically stable and can interact synergistically with supported metal nanocrystals to result in improved catalytic performances. Among various transition metal oxides, TiO_2, ZrO_2, and Al_2O_3 are often chosen as supports for metal nanocrystals owing to their high chemical stability, environmental friendliness, good reusability, and favorable synergistic effects with noble metal nanocatalysts.[21,23–25]

Commonly employed techniques for loading noble metal nanocrystals onto metal oxides include impregnation, coprecipitation, sol-gel approaches, and hydrothermal reactions.[26,27] These methods lack the ability to control the shape of noble metal nanocrystals. In addition, diffusion of metal salts into nanometer-scale pore channels is difficult during the loading process, and metal nanoparticles adsorbed close to pore openings can block the diffusion of reactant and product molecules.

Z. Jin, Dr. F. Wang, J. X. Wang, Prof. J. F. Wang
Department of Physics
The Chinese University of Hong Kong
Shatin, Hong Kong SAR, China
E-mail: jfwang@phy.cuhk.edu.hk
Dr. F. Wang, Prof. J. C. Yu
Department of Chemistry
The Chinese University of Hong Kong
Shatin, Hong Kong SAR, China

DOI: 10.1002/adfm.201202600

Therefore, the development of efficient routes for the preparation of metal oxides that are porous with high surface areas and tightly support metal nanocrystals with finely controlled shapes and compositions is highly desired in the field of catalysis. Moreover, hollow porous oxides carrying catalysts in the hollow interior brings several benefits for catalysis. First, the confined environment for chemical reactions can give enhanced catalytic reaction rates.[28,29] Second, the porous shell can strongly affect the selectivity of catalytic reactions.[30,31] Third, the low density of hollow porous oxides makes them dispersible in solutions even when large amounts of catalysts are loaded.[32] They can also be easily recovered by centrifugation or filtration.

We recently demonstrated the growth of mono- and bimetallic noble metal nanocrystals inside hollow mesoporous silica microspheres using "ship-in-a-bottle" seed-mediated growth.[33] The encapsulated metal nanocrystals can function as catalysts, exhibiting high catalytic performance. Their stability is superior to that of the corresponding unencapsulated metal nanocrystals in liquid-phase catalytic reactions. In this previous work of ours, polystyrene (PS) microspheres were utilized as the template for the coating of mesostructured silica. Calcination removed both the PS template and surfactant to generate hollow mesoporous silica microspheres. This strategy cannot be applied to the preparation of hollow mesoporous transition metal oxide microspheres, such as TiO_2 and ZrO_2, because of the difficulty in controlling the rapid hydrolysis of the oxide precursors. We have to seek other approaches for making hollow mesoporous transition metal oxide microspheres.

Aerosol-assisted self-assembly is a powerful approach for the preparation of mesoporous oxide microspheres. It combines aerosol spray and evaporation-induced self-assembly, allowing for continuous production of microspheres. Many mesoporous oxides have been made into microspheres with this method,[34–38] including SiO_2, TiO_2, ZrO_2, Al_2O_3, Cu-doped TiO_2, and $BaTiO_3$. In addition, molecular species, such as rare earth ions, organic dyes, magnetic nanoparticles, and metal salts, can be readily dissolved or dispersed in the oxide precursor solution and therefore doped into oxide microspheres to make them carry different functionalities.[25,37,39] When noble metal salts are added, calcination or H_2 reduction at raised temperatures produces metal nanoparticles that are distributed inside mesoporous oxide microspheres, as we have previously described.[25] In this method, noble metal nanoparticles are grown during the formation of mesoporous metal oxide microspheres. They generally have a spherical shape, with relatively broad size distributions. Their shape cannot be controlled. To embed multimetallic nanocrystals with complex structures, such as core/shell ones, within mesoporous oxide microspheres is also difficult.

In this work, we report on an easy-to-implement approach for the preparation of noble metal nanocrystal-embedded hollow mesoporous metal oxide microspheres through an aerosol-assisted self-assembly process. TiO_2 and ZrO_2 were chosen because of their wide uses as catalyst supports in the field of catalysis. Metal nanocrystals, including Au nanorods, Pd nanocubes, and Au core/Pd shell nanorods, were grown in advance. Therefore, their size and shape can be roughly controlled. The reduction of 4-nitrophenol (4-NP) with $NaBH_4$ to 4-aminophenol (4-AP) was selected as a model catalytic reaction to examine the catalytic performance of the Pd nanocube-embedded hollow mesoporous TiO_2 and ZrO_2 microspheres. The Pd nanocube-embedded ZrO_2 microspheres were found to exhibit good catalytic activity and recyclability. Our route offers general potential for the preparation of hollow mesoporous transition metal oxide microspheres supporting various noble metal nanocrystals for different chemical reactions.

2. Results and Discussion

The procedure for the preparation of noble metal nanocrystal-embedded hollow mesoporous oxide microspheres through the aerosol-assisted self-assembly process is illustrated schematically in **Figure 1**. Noble metal nanocrystals are first grown, followed by their adsorption to PS nanospheres. In the next step, the PS nanospheres carrying the pregrown metal nanocrystals are incorporated in mesostructured oxide microspheres through an aerosol-assisted self-assembly process. Hollow mesoporous microspheres containing the metal nanocrystals are obtained finally after calcination to remove the PS nanospheres and surfactant and at the same time crystallize the metal oxide.

In our experiments, PS nanospheres of 270 nm in diameter were utilized. They functioned simultaneously as a removable template for creating hollow interiors and as a carrier to bring pregrown noble metal nanocrystals into oxide microspheres. Noble metal nanocrystals, including Au nanorods, Pd nanocubes, and Au core/Pd shell nanorods, were chosen for the incorporation in hollow mesoporous oxide microspheres. They were grown in advance in aqueous solutions by seed-mediated growth and stabilized with cetyltrimethylammonium bromide (CTAB).[40–43] **Figure 2**A–C show the transmission electron microscopy (TEM) images of the as-grown noble metal nanocrystals. The Au nanorods have an average length of 65 ± 5 nm and diameter of 14 ± 2 nm, the Pd nanocubes have an average

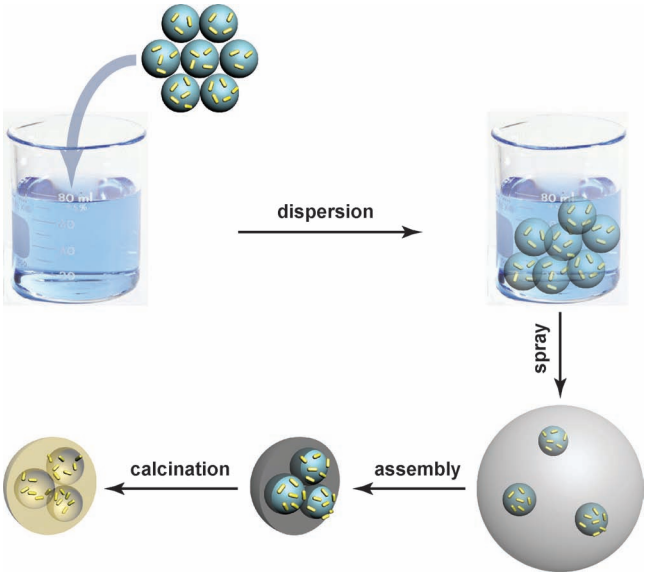

Figure 1. Schematic showing the preparation of the noble metal nanocrystal-embedded hollow mesoporous oxide microspheres through the aerosol-assisted self-assembly process.

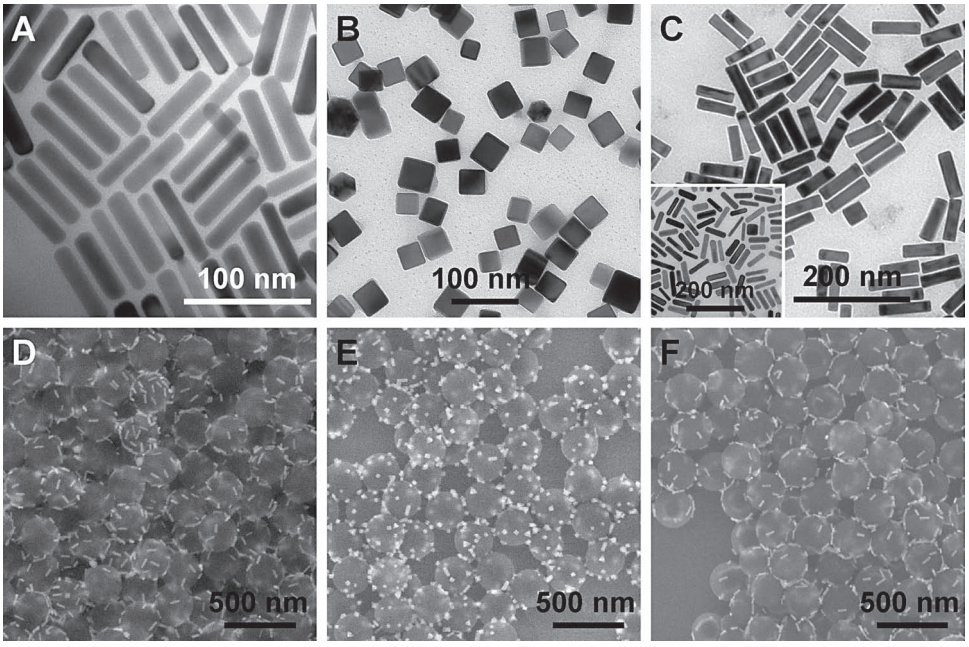

Figure 2. TEM (upper row) and SEM (lower row) images of the as-grown metal nanocrystals and the corresponding metal nanocrystals adsorbed on the PS nanospheres, respectively. A,D) Au nanorods. B,E) Pd nanocubes. C,F) Au core/Pd shell nanorods. The inset in (C) is the TEM image of the starting Au nanorods.

edge length of 34 ± 4 nm, and the Au core/Pd shell nanorods have an average length of 72 ± 6 nm and width of 20 ± 2 nm, with a Pd shell thickness around 2 nm at both the ends and side. The sizes and shapes of these metal nanocrystals are relatively uniform. They can be further synthetically varied if needed.[40–43]

The adsorption of the metal nanocrystals onto the PS nanospheres was carried out in ethanol, because the PS nanospheres are dispersible in ethanol but not water. However, the CTAB-stabilized metal nanocrystals tend to aggregate in ethanol. In order to prevent their aggregation, the capping CTAB molecules were replaced with thiol-terminated methoxypoly(ethylene glycol) (mPEG-SH, MW: 5000 g mol^{-1}). The mPEG-functionalized metal nanocrystals are dispersible in ethanol and can be readily adsorbed to the surface of the PS nanospheres through molecular interactions.[44] Figure 2D–F show the scanning electron microscopy (SEM) images of the PS nanospheres adsorbed with the Au nanorods, Pd nanocubes, and Au core/Pd shell nanorods, respectively. Each PS nanosphere carries several to several tens of the metal nanocrystals. The adsorbed metal nanocrystals are randomly distributed on the surface of the PS nanospheres. After the adsorption product was separated by centrifugation, no unadsorbed metal nanocrystals were seen under SEM imaging even over large areas (Figure S1, Supporting Information). The number of the metal nanocrystals on each PS nanosphere can be approximately controlled by varying the amount of the metal nanocrystals relative to that of the PS nanospheres.

The metal nanocrystal-decorated PS nanospheres are dispersible in the metal oxide precursor solution, which is made of metal alkoxide, acetic acid, hydrochloric acid, surfactant, and ethanol.[38] The mixture containing the PS nanospheres was transferred in an ultrasonic humidifier to generate aerosol droplets. The droplets were carried by N_2 though a horizontally aligned tube furnace set at a raised temperature, where the solvent was rapidly evaporated out of the droplets. The solvent evaporation induced simultaneously the self-assembly of the surfactant molecules and the condensation of the hydrolyzed metal oxide species.[34,36] The collected powder product was calcined to remove the PS nanospheres and surfactant as well as to crystallize the pore walls of the metal oxide microspheres. **Figure 3**A–L show the SEM and TEM images of the six types of the obtained samples that are the combinations of the three types of metal nanocrystals and the two types of transition metal oxides. The products are spheres. Their apparent morphology looks similar to that of the microspheres prepared under the same conditions without the PS nanospheres.[25,37,38] The average diameters of the TiO_2 and ZrO_2 spheres were measured from their SEM images to be 0.8 ± 0.3 μm and 0.6 ± 0.2 μm, respectively. Dark contrasts were observed on a number of the microspheres under appropriate SEM imaging conditions. We ascribe these contrasts to hollow interiors left behind after the PS nanospheres were burned away.

The presence of hollow interiors was confirmed by TEM imaging. The number percentage of the microspheres containing hollow interiors was estimated to be ≈70% by examining more than 200 microspheres under TEM imaging. One factor accounting for the absence of hollow interiors in some microspheres is the fact that some microspheres are too small to contain any hollow interiors caused by the PS nanospheres. For the oxide microspheres containing hollow interiors, the number of hollow interiors ranges from one to several, generally increasing

ADVANCED FUNCTIONAL MATERIALS
www.afm-journal.de

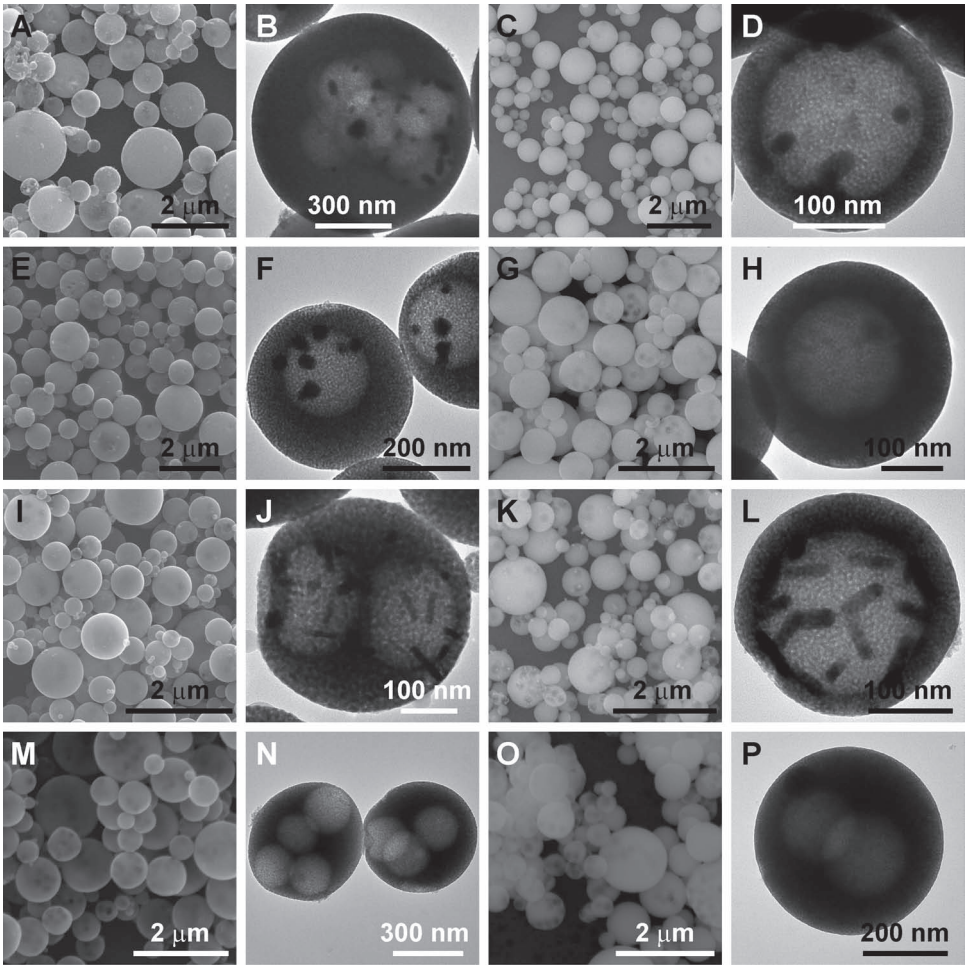

Figure 3. SEM (first and third columns) and TEM (second and fourth columns) images of the hollow mesoporous oxide microspheres. A,B) Au nanorods embedded in TiO_2. C,D) Au nanorods embedded in ZrO_2. E,F) Pd nanocubes embedded in TiO_2. G,H) Pd nanocubes embedded in ZrO_2. I,J) Au core/Pd shell nanorods embedded in TiO_2. K,L) Au core/Pd shell nanorods embedded in ZrO_2. M,N) Hollow mesoporous TiO_2 microspheres only. O,P) Hollow mesoporous ZrO_2 microspheres only.

with the diameter of the oxide microsphere. TEM imaging also reveals the presence of the metal nanocrystals inside the microspheres. The metal nanocrystals are attached to the surface of the hollow interiors. The calcination at 400 °C to remove the PS nanospheres (Figure S2, Supporting Information) also affected the shape of the metal nanocrystals. The Au nanorods were probably melted, owing to the reduction of the melting temperature of nanometer-scale metal nanocrystals,[45] or underwent surface-driven bulk reorganization,[46] and became nanospheres or largely shortened after the temperature was cooled down. In contrast, the Au core/Pd shell nanorods maintained their original shape after calcination. This thermal stability can be attributed to the protection role played by the Pd shell, because the melting point of bulk palladium is ≈500 K higher than that of bulk gold. In this regard, we reason that the Pd nanocubes also preserved their shape after calcination, although they cannot be clearly observed owing to the embedding within the hollow interiors. In comparison, the SEM and TEM images of the hollow mesoporous TiO_2 and ZrO_2 microspheres without any embedded metal nanocrystals are given in Figure 3M–P. These microspheres were prepared similarly by adding the PS nanospheres without adsorbed metal nanocrystals. The presence of the hollow interiors confirms again the templating role played by the PS nanospheres during the aerosol-assisted self-assembly process.

Our preparation method can also be readily applied to silica (Figure S3, Supporting Information). The obtained products are also microspheres, with a relatively smooth outer surface. The average diameter of the silica microspheres was measured from their SEM images to be 0.9 ± 0.3 μm. Both SEM and TEM imaging indicate the presence of hollow interiors inside the mesoporous silica microspheres. Similar to the metal nanocrystals in the TiO_2 and ZrO_2 microspheres, the Au nanorods in the silica microspheres become nanospheres or shortened, while the Au core/Pd shell nanorods maintain their shape.

We actually tried to directly disperse the pregrown metal nanocrystals in the oxide precursor solution for ultrasonic aerosol spray before the PS nanospheres were utilized. The amount

of the metal nanocrystals in the absence of the PS nanospheres was similar or even larger than that in the presence of the PS nanospheres. The CTAB-stabilized metal nanocrystals were quickly aggregated, because the oxide precursor solution contained a large volume fraction of ethanol. The mPEG-functionalized metal nanocrystals were dispersible without aggregation in the oxide precursor solution. However, the results showed that only a very small amount of the oxide microspheres, less than ≈5% in terms of the number percentage, contained the metal nanocrystals. The metal nanocrystals were found to be left behind in the sample holder of the humidifier and difficult to be carried in the droplets. These control experiments indicate the importance of using the PS nanospheres as the carrier as well as the hard template for making the metal nanocrystal-embedded hollow mesoporous oxide microspheres.

We chose the liquid-phase reduction of 4-NP by $NaBH_4$ into 4-AP as the model catalytic reaction and employed the Pd nanocube-embedded TiO_2 and ZrO_2 microspheres as the catalyst to examine the catalytic properties of the metal nanocrystal-embedded hollow mesoporous oxide microspheres (**Figure 4**A). This reaction has been widely used for evaluating the catalytic performances of various noble metal nanostructures.[47–49] The catalytic reaction takes place in the hollow interiors of the mesoporous oxide microspheres, where the metal nanocrystals are located. The mesopore channels offer the path for the diffusion of the reaction molecules between the hollow interiors and outside volume of each oxide microsphere. Moreover, the encapsulation of the metal nanocrystals within the oxide microspheres prevents the aggregation and loss of the catalyst during the reaction and recycling processes. 4-NP exhibits an absorption peak at 400 nm in alkaline solutions, while 4-AP does not exhibit any absorption peak in the visible region. The absorbance of 4-NP has a linear relationship with its concentration.[25,50,51] When $NaBH_4$ was injected into the aqueous solution of 4-NP, the color turned bright yellow, indicating the deprotonation of 4-NP. When the reduction started, the color of the reaction solution became lighter, and the absorption intensity at 400 nm dropped. At the same time, a weak absorption peak around 300 nm gradually appeared due to the absorption of 4-AP. We recorded the absorption spectra of the reaction solution as a function of the reaction time. The spectral evolution was utilized to monitor the reduction process and analyze the conversion percentage.

Figure 4B shows the time-dependent absorption spectra of the reaction solution when the Pd nanocube-embedded hollow mesoporous TiO_2 microspheres were added as the catalyst. The absorption spectra were taken at 2-min intervals after the catalyst was added. The absorption peak at 400 nm dropped gradually as the reaction time was increased. It nearly disappeared at 20 min after the reaction, indicating the completion of the reduction reaction. Since $NaBH_4$ was in large excess in the reaction, its concentration can be considered as a constant during the reduction. As a result, pseudo-first-order kinetics can be exploited with regard to the concentration of 4-NP. The concentration of 4-NP was converted from the absorbance value at 400 nm according to the predetermined calibration curve.[25] Figure 4C shows the plot of $\ln[C(t)/C(0)]$ against the reaction time, where $C(t)$ and $C(0)$ represent the concentrations of 4-NP at time t and 0, respectively. The linear fit with a coefficient of determination very close to unity supports the assumption of pseudo-first-order-kinetics. The reaction rate constant k, determined from the rate equation $\ln[C(t)/C(0)] = kt$, is 0.16 min^{-1} for the Pd nanocube-embedded TiO_2 microspheres. We also tested the catalytic activity of the Pd nanocube-embedded hollow mesoporous ZrO_2 microspheres. The time-dependent absorption spectra and plot of $\ln[C(t)/C(0)]$ against the reaction time are shown in Figure S4 of the Supporting Information. The reaction rate constant k is determined to be 0.68 min^{-1} for the ZrO_2 microspheres. The catalytic activities of the Pd nanocube-embedded TiO_2 and ZrO_2 microspheres are ascribed to the presence of the Pd nanocubes, because our

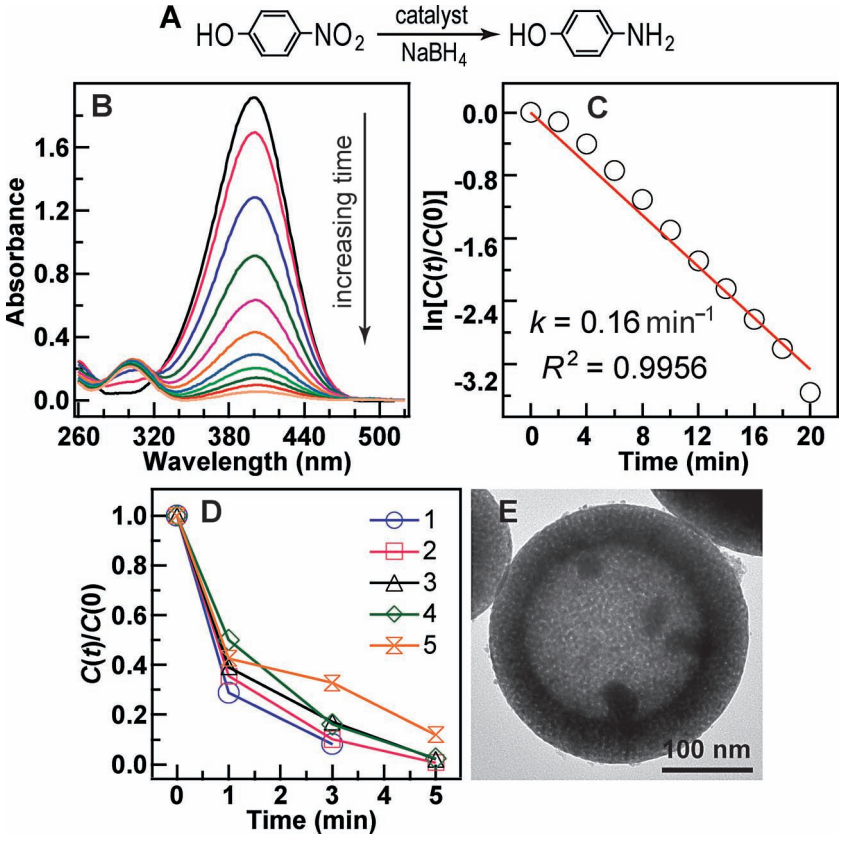

Figure 4. Catalytic reduction of 4-NP to 4-AP. A) Reaction equation. B) Time-dependent absorption spectra of the reaction solution in the presence of the Pd nanocube-embedded hollow mesoporous TiO_2 microspheres. C) Plot of $\ln[C(t)/C(0)]$ against the reaction time. The $R^2 = 0.9956$ is the coefficient of determination obtained from the linear fitting. D) Plot of $C(t)/C(0)$ against the reaction time in five successive cycles of the reduction reaction with the Pd nanocube-embedded hollow mesoporous ZrO_2 microspheres as the catalyst. E) TEM image of the ZrO_2 microspheres after five cycles of the reduction reaction.

previous experiments showed that pure TiO_2 and ZrO_2 microspheres alone cannot catalyze the reduction of 4-NP.[25]

The amounts of palladium in the two oxide microsphere catalyst samples were measured by inductively coupled plasma-atomic emission spectroscopy (ICP-AES). The mass ratios between palladium and oxide were 14×10^{-3} and 5.6×10^{-3} for the TiO_2 and ZrO_2 catalyst samples, respectively. For the catalytic reactions, the amounts of palladium contained in the hollow mesoporous TiO_2 and ZrO_2 microsphere catalysts were determined to be 1.1×10^{-8} and 2.5×10^{-9} mol, respectively. The turnover frequency (TOF), defined as the moles of reduced 4-NP molecules per mole of noble metal atoms in the oxide microsphere catalyst per minute, was employed to compare the catalytic activities of the different microsphere samples. The TOF values of the Pd nanocube-embedded TiO_2 and ZrO_2 microsphere samples were found to be 1.5 and 25 min^{-1}, respectively. The Pd nanocube-loaded ZrO_2 microspheres exhibit a higher catalytic activity. Both catalyst samples used the same Pd nanocube sample during their preparations. The difference in the TOF value is believed to result from the synergistic interaction between the Pd nanocubes and the metal oxide support. A full understanding is beyond this study. Nevertheless, our facile route to the preparation of noble metal nanocrystal-embedded hollow mesoporous oxide microspheres offers great potential for studying the synergistic interactions between different metal nanocrystals and oxide supports, as well as for discovering new, high-performance catalysts for industrially important catalytic reactions.

Beside the catalytic activity, the recyclability of catalysts is also important for their practical applications. Figure 4D shows the recyclability of the Pd nanocube-embedded ZrO_2 microsphere catalyst. Five successive cycles of the catalytic reduction were carried out. Within 5 min, more than 80% of 4-NP was reduced in all the five cycles. However, the amount of 4-NP being reduced at 5 min slightly decreased after each run. In the first four cycles, the conversion percentages were larger than 90%. In the fifth cycle, the conversion percentage dropped to 85%. The decrease in the conversion percentage is ascribed mainly to the loss of the catalyst caused by taking small amounts of the reaction solution for absorption measurements during each reaction run as well as by centrifugation after each run to collect the catalyst. TEM imaging was also performed to examine if the Pd nanocube-embedded ZrO_2 microspheres underwent reshaping or aggregation after the catalytic reactions. After five cycles, the Pd nanocubes remained embedded within the microspheres without aggregation (Figure 4E). No obvious changes can be seen under our TEM imaging conditions. The spherical shape and hollow interiors of the ZrO_2 catalyst were also preserved. These results suggest that the metal nanocrystal-embedded hollow mesoporous oxide microspheres exhibit a superior chemical and catalytic stability for the chosen liquid-phase catalytic reaction.

We further compared the catalytic activities between our Pd nanocube-embedded oxide microspheres and a commercial catalyst of palladium supported on activated charcoal (Pd/C). The amount of palladium contained in the Pd/C catalyst was adjusted to be the same as that in the hollow mesoporous ZrO_2 microsphere catalyst. The TOF value was determined to be 2.8 min^{-1} (Figure S5, Supporting Information), which was about one ninth that of the Pd nanocube-embedded ZrO_2 microsphere catalyst. The reaction rate constant k was 0.068 min^{-1}, about one tenth that of the Pd nanocube-loaded ZrO_2 catalyst. The possible factors that contribute to the superior catalytic activity of the Pd nanocube-embedded ZrO_2 microspheres include the size and shape of the Pd nanocrystals and the support. In addition, the carbon support in the Pd/C catalyst has a much smaller density, which makes the Pd/C catalyst difficult to be collected and recycled. Taken together, at the same Pd amount, our Pd nanocube-embedded ZrO_2 microspheres exhibit a much higher catalytic activity, a much larger catalytic reaction rate, and a largely improved recyclability.

3. Conclusions

We have demonstrated a general route for the preparation of noble metal nanocrystal-embedded hollow mesoporous oxide microspheres through ultrasonic aerosol spray-assisted self-assembly. PS nanospheres are employed as both the hard template for creating hollow interiors and the carrier of pregrown metal nanocrystals. The types of noble metal nanocrystals and metal oxides can be readily varied. The embedded metal nanocrystals are adsorbed on the inner surface of the hollow mesoporous oxide microspheres. The mesoporous structure of the oxide microspheres allows the access of molecular species into the hollow interiors of the oxide microspheres, where reactions catalyzed by the embedded metal nanocrystals take place. For the model catalytic reaction of reducing 4-NP by $NaBH_4$, the Pd nanocube-embedded hollow mesoporous ZrO_2 microspheres exhibit much better catalytic performances than a commercial Pd/C catalyst in terms of the catalytic activity, catalytic reaction rate, and recyclability. The approach introduced in our work can be easily extended to different metal nanocrystals. It will be useful for finding out optimal combinations of metal nanocrystals and metal oxide supports for industrially important catalytic reactions.

4. Experimental Section

Growth of the Au Nanorods: The Au nanorods were grown in aqueous solutions using a seed-mediated method.[40,41] Specifically, the preparation of the seed solution started by mixing together $HAuCl_4$ (0.01 M, 0.25 mL) and CTAB (0.1 M, 9.75 mL). A freshly prepared, ice-cold $NaBH_4$ solution (0.01 M, 0.6 mL) was then quickly injected into the mixture, followed by rapid inversion for 2 min. The resultant seed solution was kept at room temperature for 2 h before use. The growth solution was made by sequentially adding $HAuCl_4$ (0.01 M, 2 mL), $AgNO_3$ (0.01 M, 0.4 mL), HCl (0.1 M, 0.8 mL), and ascorbic acid (0.1 M, 0.32 mL) into CTAB (0.1 M, 40 mL). The resultant solution was mixed by swirling for 30 s, followed by the rapid injection of the seed solution (0.2 mL). The obtained solution was mixed by quick inversion for 2 min and thereafter kept undisturbed overnight.

Growth of the Pd Nanocubes: An oil bath was employed for the growth of the Pd nanocubes.[42] CTAB (0.1 M, 2.5 mL), deionized water (17.5 mL), and H_2PdCl_4 (0.01 M, 1 mL) were mixed in a flask, which was then kept in the oil bath preset at 80 °C for several minutes until the solution temperature was equilibrated. Ascorbic acid (0.1 M, 0.16 mL) was subsequently added into the flask. The resultant mixture solution was kept under stirring for 2 h.

Growth of the Au Core/Pd Shell Nanorods: The Au nanorods grown above were used for coating palladium to obtain the Au core/Pd shell

nanorods.[42,43] Briefly, 1 mL of the as-grown Au nanorod solution was centrifuged, the supernatant was removed, and the precipitated Au nanorods were redispersed in deionized water (1 mL) as the seeds for the Pd overgrowth. The Pd growth solution was obtained by mixing CTAB (0.1 M, 1 mL), deionized water (3 mL), H_2PdCl_4 (0.01 M, 0.02 mL), and ascorbic acid (0.1 M, 0.01 mL) together. The Au nanorod seed solution was then added into the Pd growth solution. The obtained solution was mixed by quick inversion for 2 min and subsequently kept undisturbed overnight.

Preparation of the mPEG-Stabilized Noble Metal Nanocrystals: In order to replace the capping molecules on the metal nanocrystals by mPEG-SH,[44] the as-grown metal nanocrystal solutions (Au nanorods: 40 mL, Pd nanocubes: 40 mL, Au core/Pd shell nanorods: 200 mL) were centrifuged once and redispersed in deionized water (40 mL). An aqueous mPEG-SH solution (0.01 M) was then added. The added volumes of the mPEG-SH solution were 2, 1, and 2 mL, respectively. The resultant solution was mixed by inversion for several minutes and kept undisturbed overnight.

Synthesis of the PS Nanospheres: The PS nanospheres with an average diameter of 270 nm were synthesized by polymerization of styrene with poly(vinyl pyrrolidone) (PVP, MW: 55 000 g mol^{-1}) as a steric stabilizer and 2,2′-azobis(2-methylpropionamidine) dihydrochloride (AIBA) as a radical initiator in aqueous solutions. In a typical synthesis, styrene (9.2 mL), water (90 mL), and PVP (1 g) were added to a 250-mL, three-necked, round-bottom flask equipped with a reflux condenser and a N_2 gas inlet. The air in the flask was replaced by a stream of N_2, and the mixture was kept under N_2 until the polymerization was finished. The temperature of the solution was slowly increased to 70 °C in 30 min. After that, an aqueous solution of AIBA (0.02 g mL^{-1}, 10 mL) was added into the mixture using a syringe. The polymerization reaction was carried out at 70 °C for 10 h, and the stirring rate was set at 150 rpm.

Adsorption of the Metal Nanocrystals onto the PS Nanospheres: The mPEG-functionalized metal nanocrystals (Au nanorods: 30 mL, Pd nanocubes: 40 mL, Au core/Pd shell nanorods: 30 mL) were centrifuged, the supernatant was discarded, and the precipitate was redispersed in ethanol (4 mL). The PS nanospheres (0.01 g) were then added, and the resultant mixture was kept under gentle stirring overnight. The metal nanocrystal-decorated PS nanospheres were centrifuged (7500 rpm, 15 min), and the precipitate was collected and redispersed in ethanol for the subsequent addition in the precursor solution for aerosol spray. The percentage of the metal nanocrystals that were adsorbed on the PS nanospheres was estimated to be ≈80% from the extinction spectrum of the nanocrystal solution before adsorption and that of the supernatant after adsorption. The average number of the metal nanocrystals adsorbed on each PS nanosphere was roughly controlled by the amount ratio between the metal nanocrystals and the PS nanospheres. Typically, for 0.01 g of the PS nanospheres, we found that the required volumes of the mPEG-functionalized metal nanocrystals to give appropriate numbers of the adsorbed metal nanocrystals on each PS nanosphere were 30, 40, and 30 mL for the Au nanorods, Pd nanocubes, and Au core/Pd shell nanorods, respectively. These amount ratios were used in our preparations of the metal nanocrystal-embedded hollow mesoporous oxide microspheres shown and discussed above.

Preparation of the Metal Nanocrystal-Embedded Hollow Mesoporous Oxide Microspheres: The preparation of the hollow mesoporous oxide microspheres followed our reported procedure, where no PS nanospheres were added in the precursor solution.[25,39] Specifically, to prepare the precursor solution for making the TiO_2 microspheres, triblock copolymer, $(ethylene\ oxide)_{106}$–$(propylene\ oxide)_{70}$–$(ethylene\ oxide)_{106}$ (F127, 0.6 g), was dissolved in absolute ethanol (55.4 g). In a separate beaker, titanium ethoxide (1 mL) and HCl (37 wt%, 3.2 mL) were mixed together and covered with a paraffin film. After the mixture was stirred for 2 h, the ethanolic solution of F127 was added. The resultant solution was stirred for one more hour, and then transferred to a household ultrasonic humidifier (1.7 MHz, 30 W) for aerosol spray. For the preparation of the ZrO_2 microspheres, the used amounts of the ingredients for making the precursor solution were F127 (0.26 g), absolute ethanol (25 g), zirconium butoxide (80 wt% in 1-butanol, 1 g), acetic acid (0.5 mL), and HCl (37 wt%, 0.4 mL). For the preparation of the SiO_2 microspheres, the precursor solution was made by mixing together tetraethyl orthosilicate (2.28 g, 0.01 mol), absolute ethanol (27.6 g), HCl (1 M, 0.4 mL), triblock copolymer, $(ethylene\ oxide)_{20}$–$(propylene\ oxide)_{70}$–$(ethylene\ oxide)_{20}$ (P123, 0.46 g), and deionized water (3.6 g) and kept under stirring for 1 h.[39] The metal nanocrystal-decorated PS nanospheres were added right before the precursor solution was transferred into the humidifier. The decorated PS nanospheres that were added contained 0.06–0.08 g of the PS nanospheres for all the three oxide precursor solutions. They were combined together from multiple times of the adsorption process and condensed into ethanol (4 mL) for the addition into the precursor solution. The mist generated by the ultrasonic humidifier was carried by N_2 and passed through a tube furnace set at 380 °C. The product was collected on a filter that was connected to a water aspirator. The collected microspheres were calcined at 400 °C for 5 h in air at a heating rate of 1 °C·min^{-1} to remove the surfactant and PS nanospheres.

Catalytic Reduction of 4-NP: For the catalytic reduction of 4-NP in aqueous solutions, a freshly prepared $NaBH_4$ solution (0.5 M, 0.2 mL) was added into the mixture of 4-NP (0.01 M, 0.03 mL) and deionized water (2.5 mL) in a quartz cuvette. The reaction started immediately after the metal nanocrystal-embedded hollow mesoporous oxide microsphere catalyst was added. The reduction process was monitored by measuring the absorption spectra as a function of time. The Pd amount contained in the catalyst was determined using ICP-AES. To examine the recyclability, five cycles of the reduction reactions were carried out. The reaction solution was composed of 4-NP (0.01 M, 2 mL), $NaBH_4$ (0.5 M, 2 mL), and the Pd nanocube-embedded ZrO_2 microspheres (1.78 wt%, 0.08 mL). At the end of each run, the microspheres were collected by centrifugation and redispersed in a fresh reaction solution. During each run, a small amount of the reaction solution (0.05 mL) was taken out at 1, 3, and 5 min for the measurements of the absorption spectra. The Pd/C catalyst containing 5 wt% of palladium was purchased from Aladdin, Shanghai, China. It appeared as black powder.

Characterization: SEM images were acquired on an FEI Quanta 400 FEG microscope. TEM images were obtained on an FEI CM120 microscope at 120 kV. Thermogravimetric analysis traces were recorded on a PerkinElmer TAG6 system. Absorption and extinction spectra were recorded using a Hitachi U-3501 UV/visible/NIR spectrophotometer. ICP-AES measurements were made on a PerkinElmer Optima 4300DV system.

Supporting Information

Supporting Information is available from the Wiley Online Library or from the author.

Acknowledgements

The second author is in the Department of Physics. The third author is in the Department of Chemistry. This work was supported by the Research Grants Council of Hong Kong (NSFC/RGC Joint Research Scheme, Ref. No.: N_CUHK465/09, Project Code: 2900339).

Received: September 9, 2012
Published online: November 22, 2012

[1] A. R. Tao, S. Habas, P. D. Yang, *Small* **2008**, *4*, 310–325.
[2] Y. N. Xia, Y. J. Xiong, B. Lim, S. E. Skrabalak, *Angew. Chem. Int. Ed.* **2009**, *48*, 60–103.
[3] B. Lim, M. J. Jiang, J. Tao, P. H. C. Camargo, Y. M. Zhu, Y. N. Xia, *Adv. Funct. Mater.* **2009**, *19*, 189–200.

[4] H. Zhang, M. S. Jin, Y. N. Xia, *Angew. Chem. Int. Ed.* **2012**, *51*, 7656–7673.
[5] K. M. Bratlie, H. Lee, K. Komvopoulos, Y. D. Yang, G. A. Somorjai, *Nano Lett.* **2007**, *7*, 3097–3101.
[6] N. Tian, Z. Y. Zhou, S.-G. Sun, Y. Ding, Z. L. Wang, *Science* **2007**, *316*, 732–735.
[7] C.-L. Lu, K. S. Prasad, H.-L. Wu, J. A. Ho, M. H. Huang, *J. Am. Chem. Soc.* **2010**, *132*, 14546–14553.
[8] F. Wang, C. H. Li, L.-D. Sun, H. S. Wu, T. Ming, J. F. Wang, J. C. Yu, C.-H. Yan, *J. Am. Chem. Soc.* **2011**, *133*, 1106–1111.
[9] F. Wang, C. H. Li, L.-D. Sun, C.-H. Xu, J. F. Wang, J. C. Yu, C.-H. Yan, *Angew. Chem. Int. Ed.* **2012**, *51*, 4872–4876.
[10] W. O. Oduro, N. Cailuo, K. M. K. Yu, H. W. Yang, S. C. Tsang, *Phys. Chem. Chem. Phys.* **2011**, *13*, 2590–2602.
[11] W. Chrzanowski, A. Wieckowski, *Langmuir* **1998**, *14*, 1967–1970.
[12] J. R. C. Salgado, E. Antolini, E. R. Gonzalez, *J. Phys. Chem. B* **2004**, *108*, 17767–17774.
[13] J. B. Wu, J. L. Zhang, Z. M. Peng, S. C. Yang, F. T. Wagner, H. Yang, *J. Am. Chem. Soc.* **2010**, *132*, 4984–4985.
[14] C. Ramarao, S. V. Ley, S. C. Smith, I. M. Shirley, N. DeAlmeida, *Chem. Commun.* **2002**, 1132–1133.
[15] K. Okamoto, R. Akiyama, H. Yoshida, T. Yoshida, S. Kobayashi, *J. Am. Chem. Soc.* **2005**, *127*, 2125–2135.
[16] E. H. Rahim, F. S. Kamounah, J. Frederiksen, J. B. Christensen, *Nano Lett.* **2001**, *1*, 499–501.
[17] J. K. Cho, R. Najman, T. W. Dean, O. Ichihara, C. Muller, M. Bradley, *J. Am. Chem. Soc.* **2006**, *128*. 6276–6277.
[18] J. P. Ge, T. Huynh, Y. X. Hu, Y. D. Yin, *Nano Lett.* **2008**, *8*, 931–934.
[19] S. H. Joo, J. Y. Park, C.-K. Tsung, Y. Yamada, P. D. Yang, G. A. Somorjai, *Nat. Mater.* **2009**, *8*, 126–131.
[20] J. K. Edwards, B. Solsona, E. Ntainjua N, A. F. Carley, A. A. Herzing, C. J. Kiely, G. J. Hutchings, *Science* **2009**, *323*, 1037–1041.
[21] J. H. Kwak, J. Z. Hu, D. H. Mei, C.-W. Yi, D. H. Kim, C. H. F. Peden, L. F. Allard, J. Szanyi, *Science* **2009**, *325*, 1670–1673.
[22] Y. Yamada, C.-K. Tsung, W. Y. Huang, Z. Y. Huo, S. E. Habas, T. Soejima, C. E. Aliaga, G. A. Somojai, P. D. Yang, *Nat. Chem.* **2011**, *3*, 372–376.
[23] J. K. Edwards, E. Ntainjua N, A. F. Carley, A. A. Herzing, C. J. Kiely, G. J. Hutchings, *Angew. Chem. Int. Ed.* **2009**, *48*, 8512–8515.
[24] I. Lee, J. B. Joo, Y. D. Yin, F. Zaera, *Angew. Chem. Int. Ed.* **2011**, *50*, 10208–10211.
[25] Z. Jin, M. D. Xiao, Z. H. Bao, P. Wang, J. F. Wang, *Angew. Chem. Int. Ed.* **2012**, *51*, 6406–6410.
[26] J. Hagen, *Industrial Catalysis: A Practical Approach*, Wiley-VCH, Weinheim, Germany **2006**, pp 223–237.
[27] G. A. Somorjai, J. Y. Park, *Top. Catal.* **2008**, *49*, 126–135.
[28] S. M. Leeder, M. R. Gagné, *J. Am. Chem. Soc.* **2003**, *125*, 9048–9054.
[29] Y. Yamada, M. Mizutani, T. Nakamura, K. Yano, *Chem. Mater.* **2010**, *22*, 1695–1703.
[30] L. Pan, H. M. Liu, X. G. Lei, X. Y. Huang, D. H. Olson, N. J. Turro, J. Li, *Angew. Chem. Int. Ed.* **2003**, *42*, 542–546.
[31] E. Kockrick, T. Lescouet, E. V. Kudrik, A. B. Sorokin, D. Farrusseng, *Chem. Commun.* **2011**, *47*, 1562–1564.
[32] S. D. Miao, C. L. Zhang, Z. M. Liu, B. X. Han, Y. Xie, S. J. Ding, Z. Z. Yang, *J. Phys. Chem. C* **2008**, *112*, 774–780.
[33] M. D. Xiao, C. M. Zhao, H. J. Chen, B. C. Yang, J. F. Wang, *Adv. Funct. Mater.* **2012**, *22*, 4526–4532.
[34] Y. F. Lu, H. Y. Fan, A. Stump, T. L. Ward, T. Rieker, C. J. Brinker, *Nature* **1999**, *398*, 223–226.
[35] G. V. R. Rao, G. P. López, J. Bravo, H. Pham, A. K. Datye, H. F. Xu, T. L. Ward, *Adv. Mater.* **2002**, *14*, 1301–1304.
[36] D. Grosso, G. J. A. A. Soler-Illia, E. L. Crepaldi, B. Charleux, C. Sanchez, *Adv. Funct. Mater.* **2003**, *13*, 37–42.
[37] L. Li, C.-K. Tsung, Z. Yang, G. D. Stucky, L. D. Sun, J. F. Wang, C. H. Yan, *Adv. Mater.* **2008**, *20*, 903–908.
[38] C.-K. Tsung, J. Fan, N. F. Zheng, Q. H. Shi, A. J. Forman, J. F. Wang, G. D. Stucky, *Angew. Chem. Int. Ed.* **2008**, *47*, 8682–8686.
[39] L. Li, C.-K. Tsung, T. Ming, Z. H. Sun, W. H. Ni, Q. H. Shi, G. D. Stucky, J. F. Wang, *Adv. Funct. Mater.* **2008**, *18*, 2956–2962.
[40] W. H. Ni, K. S. Kou, Z. Yang, J. F. Wang, *ACS Nano* **2008**, *2*, 677–686.
[41] T. Ming, X. S. Kou, H. J. Chen, T. Wang, H.-L. Tam, K.-W. Cheah, J.-Y. Chen, J. F. Wang, *Angew. Chem. Int. Ed.* **2008**, *47*, 9685–9690.
[42] F. Wang, L.-D. Sun, W. Feng, H. J. Chen, M. H. Yeung, J. F. Wang, C.-H. Yan, *Small* **2010**, *6*, 2566–2575.
[43] Y. J. Xiang, X. C. Wu, D. F. Liu, X. Y. Jiang, W. G. Chu, Z. Y. Li, Y. Ma, W. Y. Zhou, S. S. Xie, *Nano. Lett.* **2006**, *6*, 2290–2294.
[44] M. D. Xiao, H. J. Chen, T. Ming, L. Shao, J. F. Wang, *ACS Nano* **2010**, *4*, 6565–6572.
[45] K. Dick, T. Dhanasekaran, Z. Y. Zhang, D. Meisel, *J. Am. Chem. Soc.* **2002**, *124*, 2312–2317.
[46] Y. T. Wang, S. Teitel, C. Dellago, *Nano Lett.* **2005**, *5*, 2174–2178.
[47] J. Lee, J. C. Park, H. Song, *Adv. Mater.* **2008**, *20*, 1523–1528.
[48] J. P. Ge, Q. Zhang, T. R. Zhang, Y. D. Yin, *Angew. Chem. Int. Ed.* **2008**, *47*, 8924–8928.
[49] J. Zeng, Q. Zhang, J. Y. Chen, Y. N. Xia, *Nano Lett.* **2010**, *10*, 30–35.
[50] K. Hayakawa, T. Yoshimura, K. Esumi, *Langmuir* **2003**, *19*, 5517–5521.
[51] S. Praharaj, S. Nath, S. K. Ghosh, S. Kundu, T. Pal, *Langmuir* **2004**, *20*, 9889–9892.